

Future Global and Regional Human Exposure to Tropical Night Heat Events

G. T. Jordan^{1*} and C. M. Brierley¹

¹Dept of Geography, University College London, Gower St, London, U.K.

Key Points:

- The number of tropical nights (those with minimum temperatures above 20°C) was explored in the CMIP6 scenarios
- Tropical nights increase in all future scenarios for all regions of the globe, as does the population exposed to them.
- Much of this increased extreme heat exposure could be avoided by stringent climate mitigation measures.

*Current address, UK Met. Office

Corresponding author: G. T. Jordan, george.jordan@metoffice.gov.uk

Corresponding author: C. Brierley, c.brierley@ucl.ac.uk

Abstract

Extreme heat events are one of the most dangerous climate hazards and they are projected to increase in frequency, intensity and duration as this century progresses. Change in future exposure to extreme heat events depends not only on climate change, but also on changes to future population size and the areas this population inhabits. This study explores exposure to the heat event known as a tropical night. Using a CMIP6 multi-model ensemble, coupled with population projections, this study projects exposure for the four alternative futures described by SSP1-2.6, SSP2-4.5, SSP3-7.0, and SSP5-8.5. Exposure is quantified annually at both the global and regional scale, relative to a pre-industrial baseline. By the end of the twenty-first century global annual exposure to tropical nights will total 1338-2674 billion person-days depending on the pathway followed. Of the four pathways, globally change in exposure from the pre-industrial is avoided most under SSP1-2.6, which, when compared to SSP3-7.0 which projects the greatest change, is a reduction of 1336 billion person-days annually. Exposure reduction varies at the regional level, yet in the majority of cases, SSP1-2.6 remains the more desirable future in terms of minimising future exposure. Moreover, this study finds that changes in climate versus changes in population do not equally influence changes in exposure, and their contributions vary regionally. Irrespective of the future pathway followed, human exposure is set to increase at the global scale and for the vast majority of regions.

Plain Language Summary

Extreme heat is a substantial health risk, and the amount of people exposed to it is expected to increase with climate change. One measure of extreme heat is when the temperature at night does not fall below 20°C, because this prevents the body recovering from heat stress suffered during the day. Using a collection of new model projections, we look at the impact of climate change on this measure. Unsurprisingly more places experience extreme heat, and more often, as the climate warms. We combine this with scenarios of future population to look at where and when people are exposed to these dangerous night-time conditions. We show that much of this risk could be avoided by keeping global warming in check.

1 Introduction

The profound socioeconomic implications of extreme climate events cannot fail to grab humanity's attention. These calamities affect the health of both our physiology and economies, often decimating agricultural yields and labour productivity, disrupt our social structures, at times forcing migration, as well as aggravating many other areas in a myriad of complex ways (Carleton & Hsiang, 2016). Extreme climate events are rare, with characteristics defined by the tails of probability distributions (Visser & Petersen, 2012), yet increasing media coverage of the devastation they inflict has prompted a surge in societal interest (Karl & Easterling, 1999; Boudet et al., 2020; Hopke, 2020). It has long since been reported that a changing climate will alter the intensity, frequency, duration, and geographic extent of these events (Mearns et al., 1984; Wigley, 1985, 2009), yet quantifying such change is difficult, primarily due to their rarity (Nicholls, 1995; Frei & Schar, 2001). Increasing acceptance that anthropogenic climate change is a reality has generated a great deal of attention towards its effect on extreme events and there now exists ever-growing evidence that human activity is modifying them, especially those of extreme heat (Peterson et al., 2012, 2013; Stott et al., 2014; Herring et al., 2015, 2016, 2018, 2019, 2020). To advance this effort, this study will explore humanity's exposure to extreme heat during the pre-industrial, present day, and end of the twenty-first century using state-of-the-art climate and population projections.

An extreme heat event, often termed a heat wave, is a prolonged period of high temperatures exceeding the local average at a given time. The beginning of the twenty-first

century saw numerous extreme heat events causing a significant impact upon ecosystems, societies, and economies. For example, communities across Europe in 2003 and Russia in 2010 suffered 70,000 and 55,000 heat-related deaths respectively, revealing the infamous relationship between extreme heat and mortality (Robine et al., 2008; Barriopedro et al., 2011). Furthermore, a 2013 heat event across eastern China saw fierce economic consequences due to its impact on agriculture and infrastructure, culminating in an estimated direct loss of 59 billion RMB (Sun et al., 2014). Similarly, extreme heat events place considerable strain on utility services. For instance, in 2015, a two-day heat event across England led to emergency speed restrictions across the national rail network resulting in 220,000 minutes of delays (Ferranti et al., 2018). In like manner, between 2006-2013, Buenos Aires experienced 20 extreme heat-related power blackouts leaving millions without electricity (Santagata et al., 2017). Also of significance are the impacts on ecosystems caused by extreme heat. For example, in 2011 the Australian west coast experienced a marine heat event which catalysed a local bio-diversity shift towards warm water fish species permanently changing this ecosystem and the services it provides (Wernberg et al., 2013). These examples are noted here to provide a glimpse of the range of consequences extreme heat can cause with more detailed views provided by Perkins (2015), Carleton and Hsiang (2016), and Horton et al. (2016). Clearly extreme heat events have severe ramifications making this study's contribution in understanding them imperative.

1.1 Historical Trends

Since the turn of the century, extreme heat event research has increased considerably, focusing mainly on their intensity, frequency, and duration. The Fifth Assessment Report of the Intergovernmental Panel on Climate Change (AR5 IPCC) concluded that since the mid-twentieth century it is likely ($\geq 66\%$ probability) that the frequency of heat events has increased in large parts of Europe, Asia, and Australia (IPCC, 2013). Since then, more studies of these regions have emerged supporting, not only increases in heat event frequency, yet also increases in their intensity and duration (Rahmstorf & Coumou, 2011; Donat et al., 2014; Mishra et al., 2015; Luo & Lau, 2017; Founda et al., 2019; Luo et al., 2020). For example, a study using daily temperature observations between 1950-2011 by Perkins et al. (2012), concluded that, for a given year, the maximum temperature of its most intense heat event grew on average by 2.0°C, 0.8-1.0°C, and 0.4-0.8°C per decade across East Asia, Europe, and Australia respectively. Furthermore, such trends are not limited to these regions. For instance, Ceccherini et al. (2017) state that the average annual number of African extreme heat events between 2006-2015 was 24.5, double that of its value between 1981-2005. This study also reports increases, albeit of smaller magnitude, in the duration and intensity of heat events, as found in other African studies (Fontaine et al., 2013; Moron et al., 2016). Indeed, these trends are also reported in North America. For example, DeGaetano and Allen (2002) found that between 1960-1996 the number of times that daily maximum temperature exceeded the 95th percentile increased, and consequently infer an increase in heat event frequency and intensity across this period. Conversely, a separate North America study using a different heat event definition, concludes that southeastern North America does not exhibit these trends (Alexander et al., 2006). Additionally, in South America, Ceccherini et al. (2016) reported that heat event intensity and frequency has increased since 1980, with the greatest increases occurring post 2000. However, other studies suggests that these increases are true only for heat events defined using daily minimum temperatures, and that, for instance, in southern South America there are no significant trends across 1980-2010 (Alexander et al., 2006; Rusticucci, 2012; Mishra et al., 2015). In summary, globally most land areas have experienced more intense, frequent, and longer heat events since the mid-twentieth century, with only a few regions, such as southern South America and southeastern North America, failing to exhibit such trends. Where discrepancies do exist in select regions, the studies often employ differing heat event definitions. Hence, this study will be ex-

licit in defining a heat event and cautious with comparison to literature employing alternative definitions.

1.2 Future Projections

Coupled atmosphere-ocean general circulation models (GCMs) and Earth system models (ESMs) are frequently used in future extreme heat event research. The projections used are predominately those made for the Coupled Model Intercomparison Project (CMIP, (Meehl et al., 2005, 2007; Taylor et al., 2012)). As each CMIP phase uses differing emissions scenarios, this summary will reference a scenario as high, medium, or low relative to others of the same phase. The latest IPCC assessment found that it is very likely (90-100% probability) that future heat events will occur with greater frequency and duration (IPCC, 2013), and global studies since, despite their scarcity, further support this (Coumou & Robinson, 2013; Russo et al., 2014; Dosio et al., 2018). For example, Fischer and Knutti (2015) found that, under future 2°C warming, by 2050 the probability of an extreme heat event, defined as exceeding the 99th percentile, is over five times higher than that of the pre-industrial. Equally, Sillmann, Kharin, Zwiers, et al. (2013) found that by the end of the twenty-first century, the global annual number of heat days on land, defined as those exceeding the 90th percentile of 1961-1990, will increase by 167 days under a high emissions scenario. In regard to the far greater quantity of regional studies, those focused on the Mediterranean present striking projections (Amengual et al., 2014; Lelieveld et al., 2014; Viceto et al., 2019). For example, Seneviratne et al. (2016) project that under present day warming of 2°C, the magnitude of the most extreme Mediterranean heat events will still rise by 3°C. Indeed, Cardoso et al. (2019) concluded that, under a high emissions scenario, half of the end of the twenty-first century Portuguese heat events will be stronger than the notorious European 2003 heat event and will last 17 days longer than those of 1971-2000. Additionally, Asian heat events are projected to be more intense, frequent, and longer. For instance, by 2050 under a high emissions scenario, South Korea is projected a 131% increase in heat events above 30°C and a 50% reduction in their inter-annual variability relative to 1981-2005 (Lee et al., 2014). Similarly, in India, only under a low emissions scenario will changes in heat events, defined as consecutive days exceeding 45°C, be avoided in the populous southern regions (Murari et al., 2014). Finally, increases in frequency, intensity, and duration are projected for Australian (Cowan et al., 2014) and South American (Feron et al., 2019) heat events, with greatest change occurring in their respective northern regions. In short, the literature projects more intense, common, and longer heat events, with increases more substantial under higher emissions scenarios. In order to benefit from the latest CMIP6 phase (Eyring et al., 2016) and address the need for global scale analysis, this study will explore heat events both globally and regionally under the new emissions pathways.

2 Data and Methods

This study uses daily minimum surface temperatures output from 15 climate models developed by various institutes around the world. The CMIP6 historical simulations provide data for the pre-industrial and present day (Eyring et al., 2016), whereas the SSP1-2.6, SSP2-4.5, SSP3-7.0, and SSP5-8.5 scenarios from the Scenario Model Intercomparison Project (ScenarioMIP) provide end of the twenty-first century data (O'Neill et al., 2016). Although some models have multiple members, this study uses a single member for each model, typically r1i1p1f1, as the influence of internal model variability on extreme heat event metrics is relatively low compared to that of physically different models (Perkins-Kirkpatrick & Gibson, 2017). Each model in Table 1 is chosen based on having at least one member with daily minimum surface temperature data available for both the CMIP6 historical simulations and ScenarioMIP as of June 2020 (the start of this work). Monthly ('tas') and daily minimum temperatures ('tasmin') are used to generate average annual temperatures and average annual extreme heat metrics respectively. Anoma-

Model	Institution Initials	Country	Atmospheric Resolution (Lat. x Lon.)	Reference
ACCESS-CM2 ^a	CSIRO- ARCCSS	Australia	1.25°x 1.88°	Law et al. (2017)*
ACCESS-ESM1-5 ^b	CSIRO	Australia	1.25°x 1.88°	Law et al. (2017)*
AWI-CM-1-1-MR ^a	AWI	Germany	0.93°x 0.94°	Semmler et al. (2020)
BCC-CSM2-MR ^a	BCC	China	1.13°x 1.13°	Wu et al. (2019)
CanESM5 ^b	CCCma	Canada	2.81°x 2.81°	Swart et al. (2019)
CNRM-CM6-1 ^a	CNRM- CERFACS	France	1.41°x 1.41°	Voldoire et al. (2019)
GFDL-ESM4 ^b	NOAA- GFDL	USA	1.00°x 1.25°	Dunne et al. (2020)
INM-CM4-8 ^a	INM	Russia	1.50°x 2.00°	Volodin et al. (2018)
INM-CM5-0 ^a	INM	Russia	1.50°x 2.00°	Volodin et al. (2017)
IPSL-CM6A-LR ^a	IPSL	France	1.26°x 2.50°	Boucher et al. (2020)
MIROC6 ^b	MIROC	Japan	1.41°x 1.41°	Tatebe et al. (2019)
MPI-ESM1-2-HR ^b	MPI-M	Germany	0.94°x 0.94°	Muller et al. (2018)
MRI-ESM2-0 ^b	MRI	Japan	1.13°x1.13°	Yukimoto et al. (2019)
NorESM2-MM ^b	NCC	Norway	0.94°x 1.25°	Seland et al. (2020)
UKESM1-0-LL ^b	MOHC	UK	1.25°x 1.88°	Sellar et al. (2019)

Table 1: Model names, modelling institutions and countries, and atmospheric resolutions of 15 CMIP6 climate models. Model names denoted with a and b are GCMs and ESMs respectively. *Previous model version reference.

lies represent deviations from their corresponding 50-year pre-industrial baselines. Processing these average variables involve time averaging in a model's native grid before using bilinear interpolation to a common 1.0° x 1.0° latitude-longitude grid for use with population projections and model evaluation. This study primarily focuses on multi-model ensemble output as they have been shown to outperform individual models (Tebaldi & Knutti, 2007). All models will be weighted equally when forming a multi-model ensemble as, although some models will outperform others when compared to observations, this is not necessarily a precursor for success in simulating climates absent of observations (Knutti et al., 2007). Regional analysis, including determining the mean, median, and various percentiles, is performed on the common grid for IPCC AR6 scientific land regions, excluding those covering Antarctica (Iturbide et al., 2020).

2.1 Heat Event and Exposure Definitions

As a universal heat event definition remains an open research question, this study employs one it deems most appropriate. For a given day, a heat event will be said to occur if the daily minimum temperatures exceeds 20°C. This is commonly referred to as a tropical night (TR). The use of an absolute threshold, specifically a minimum one, ensures only heat events genuinely dangerously warm are considered by guaranteeing a minimum intensity. This study acknowledges that relative threshold definitions can account for local heat acclimatisation yet does not deem it suitable for use with future scenarios where the underlying socioeconomic factors, and subsequently the ability to adapt to heat, for a given region can differ. The number tropical nights per year is averaged over the relevant climatological period (1851-1900 for the pre-industrial, 1981-2010 for the ‘present day’, and 2071-2100 for the end of the twenty-first century). As the average annual count of tropical nights ($TR_{\bar{A}}$) has fixed maximum and minimum values, using bilinear interpolation during processing is appropriate as it is monotonic.

To determine human exposure to TRs for a given period, climate projections are combined with population projections on a common 1.0° x 1.0° latitude-longitude grid. For each cell, the annual TR count is multiplied by the projected population returning a gridded exposure distribution of annual heat exposure measured in person-days. As exposure is calculated at the grid cell level, for this study’s global and regional analysis, exposure is aggregated accordingly.

2.2 Model Evaluation

Following previous CMIP studies of climate extreme indices, this study uses root mean square error (RMSE) metrics to assess model performance against observations for the present day (Gleckler et al., 2008; Sillmann, Kharin, Zhang, et al., 2013). Using a set of model RMSEs, the relative RMSE of model i , $RMSE_{ij}^R$, for observational dataset j is given by

$$RMSE_{ij}^R = \frac{RMSE_{ij} - RMSE_j^M}{RMSE_j^M} \quad (1)$$

where $RMSE_j^M$ is the median RMSE of the set of models compared with observation dataset j . This median RMSE is not equivalent to the multi-model ensemble RMSE which this study also computes. The observational dataset used for average annual temperature RMSEs is the 5.0° x 5.0° latitude-longitude CRUTEM4 land-surface air temperature dataset (Osborn & Jones, 2014), whereas the 2.5° x 3.75° latitude-longitude HadEX2 extreme indices dataset is used for $TR_{\bar{A}}$ RMSEs (Donat et al., 2013). Bilinear interpolation is used to translate both model outputs to the coarser native resolutions of the observational datasets. Both sets of observations lack full spatial coverage due to station-data scarcity, particularly across Africa, South America and the polar regions. Consequently, the global RMSEs of this study only consider the land regions present in each observational dataset.

2.3 Historical Population Projections

HYDE 3.2 population projections cover a period from 10,000 BC to 2015, with data for 1700-2000 and 2000-2015 available at decadal and annual intervals respectively. The projections include counts of total, urban, and rural populations, and are frequently utilised in other climate research (e.g. Newbold et al. (2015); Searchinger et al. (2018); Pugh et al. (2019)). To obtain spatial distributions, HYDE 3.2 uses various population time series of areas defined by current country boundaries and subjects them to a weighting algorithm centred on habitat suitability. In doing so, population estimates are distributed

across a $0.083^\circ \times 0.083^\circ$ latitude-longitude grid based on the likelihood a given grid cell is inhabited (Goldewijk et al., 2010). This study computes equally weighted time-averages of these distributions using the decadal projections across 1850-1900 and 1980-2010 for the pre-industrial and current period respectively. Doing so potentially undervalues the exponential population changes seen between 1980-2010, yet is necessary as to keep with the conventional 30-year window used in climate studies. A pre-industrial anomaly for the present day is computed where each anomaly represents the deviation from the 50-year mean pre-industrial population at a particular grid cell. All time-averaged projections are translated to a common $1.0^\circ \times 1.0^\circ$ latitude-longitude grid for use with climate projections by summing the population counts that fall within each 1.0° grid cell. Regional projections for the IPCC AR6 scientific land regions (Iturbide et al., 2020) are computed similarly.

2.4 Future Population Projections

The NCAR-CIDR projections provide population distributions for each SSP which are consistent with their underlying demographic assumptions and exhibit the population dynamics inferred within their narratives. The population projections cover the period 2010-2100 in decadal time steps at a $0.125^\circ \times 0.125^\circ$ latitude-longitude resolution and are increasingly used in current climate research (e.g. Zhang et al. (2017); Dottori et al. (2018); W. Liu et al. (2018)). Each projection consists of total, urban, and rural population counts. Quantitatively each projection is consistent at the national level as the total, urban, and rural population counts are constrained to equal those of the SSP for every nation. Also, the projections are qualitatively consistent as the demographic characteristics of each narrative are translated into model parameters related to urban and rural population development (Jones & O'Neill, 2013, 2016). This study computes equally weighted time-averages of the 2070-2100 decadal NCAR-CIDR projections for SSP1, SSP2, SSP3, and SSP5, as well as anomalies relative to the pre-industrial baseline from HYDE 3.2 projections. Due to differing resolutions, the latter is computed on a common $1.0^\circ \times 1.0^\circ$ latitude-longitude grid. The methods used for the translation to this common grid and computing regional values are the same as that of the historical projections.

3 Results

3.1 Model Performance

The individual model and multi-model ensemble performances in projecting present day $TR_{\bar{A}}$ versus HadEX2 observations are displayed in Figure 1 and 2. Generally the individual models tend to overestimate $TR_{\bar{A}}$ in regions of South America, Africa, Australia, and western North America by over 45 days, whereas most underestimate $TR_{\bar{A}}$ in the Northern Hemisphere by 1-5 days. Nevertheless, some models outperform others as evident through the RMSE metrics, with IPSL-CM6A-LR and INM-CM4-8 performing best, and MIROC6, AWI-CM-1-1-MR, and MPI-ESM1-2-HR, the worst. Interestingly two of the worst performers, AWI-CM-1-1-MR, and MPI-ESM1-2-HR, have the finest resolutions, suggesting that a finer resolution does not necessarily equal better $TR_{\bar{A}}$ projections. Lastly, the multi-model ensemble largely outperforms the individual models with its relative RMSE only surpassed by IPSL-CM6A-LR and INM-CM4-8. In short, individual model performance in projecting $TR_{\bar{A}}$ is varied, whereas the multi-model ensemble consistently outperforms most.

3.2 Tropical Nights

Clear global patterns in annual mean surface temperature change exist across projections (Figure 3). As well as projecting the greatest warming at the global scale, SSP5-

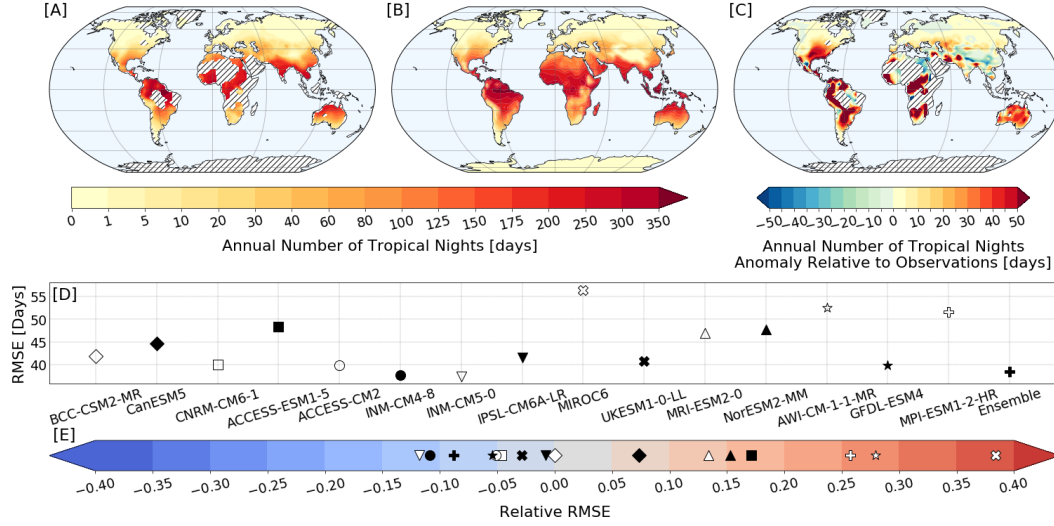


Figure 1: Present day (1981-2010) average annual number of tropical nights derived from [A] HadEX2 observations and [B] CMIP6 multi-model ensemble simulations, along with [C] the multi-model ensemble observational anomaly. Hatched areas lack observational data. Ocean areas are masked for clarity. [D-E] RMSE performance metrics for both the multi-model ensemble and its individual members.

8.5 does so for all 44 AR6 regions, with the largest pre-industrial anomalies of 9.51°C and 8.88°C found in RAR (Russian Arctic) and NEN (northeastern North America). Interestingly, the third largest anomaly of 8.01°C is for RAR under SSP3-7.0, a lower GHG concentration scenario, highlighting the severity of warming projected for this region. Conversely, for all 44 regions, SSP1-2.6 avoids the most future warming, with the lowest pre-industrial change of 1.39°C projected for SSA (southern South America), followed by 1.55°C and 1.69°C for NZ (New Zealand) and SAU (southern Australia) respectively. Similarly, regions with annual mean temperatures $> 30.0^{\circ}\text{C}$ can be avoided entirely under SSP1-2.6, whereas 5 exist under SSP5-8.5. Importantly, a decrease in annual mean temperature from the present day is not projected for any region by the end of the twenty-first century. Finally, the multi-model ensemble mean is greater than the median for most regions, indicating a positively skewed distribution, with this skew more apparent under SSP3-7.0 and SSP5-8.5, than SSP1-2.6, and SSP2-4.5. In short, the greatest avoidance in future warming from the pre-industrial, both globally and regionally, is under SSP1-2.6.

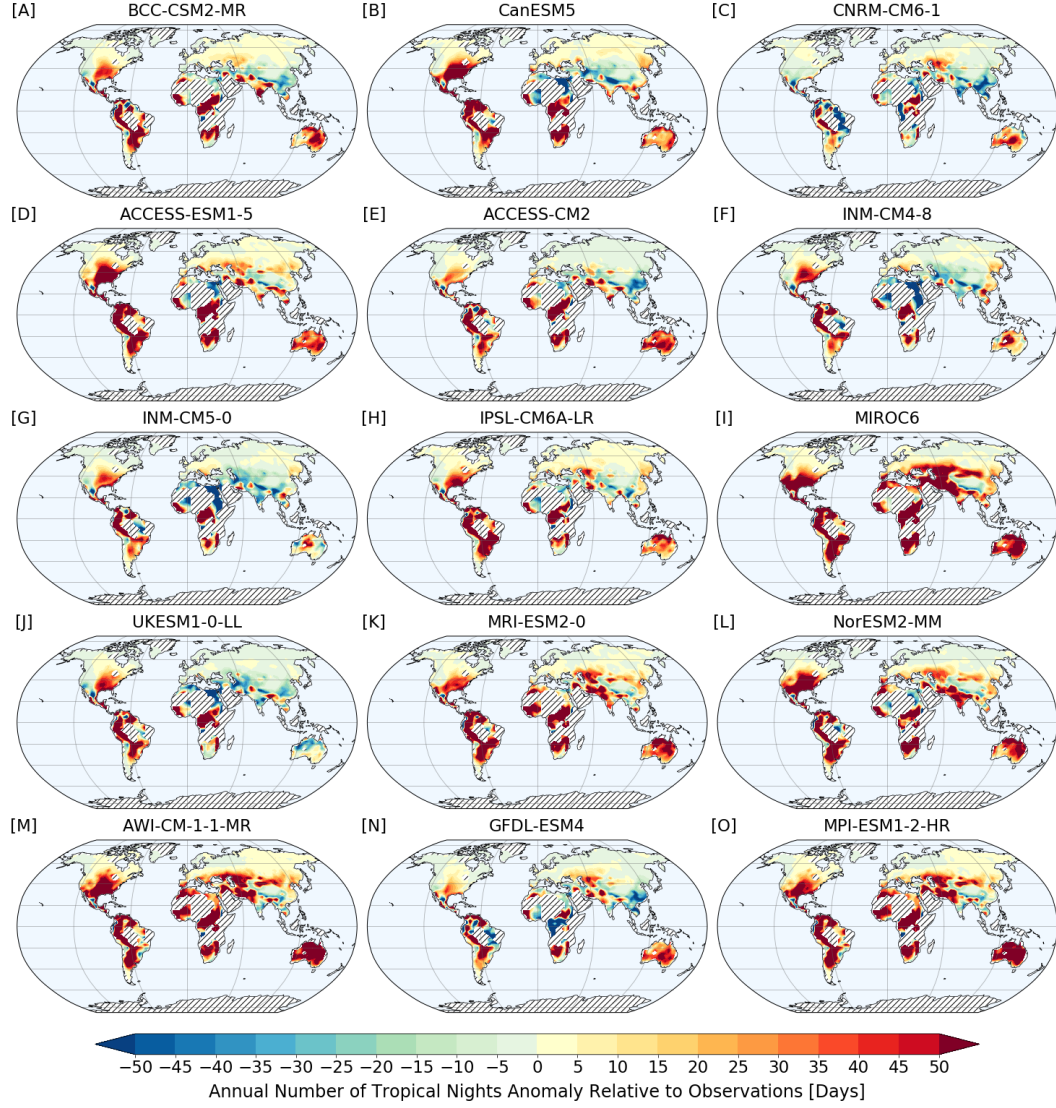


Figure 2: Average annual number of tropical nights present day (1981-2010) projection anomaly relative to those of HadEX2 observations for 15 CMIP6 models. Hatched areas lack observational data. Ocean area are masked for clarity.

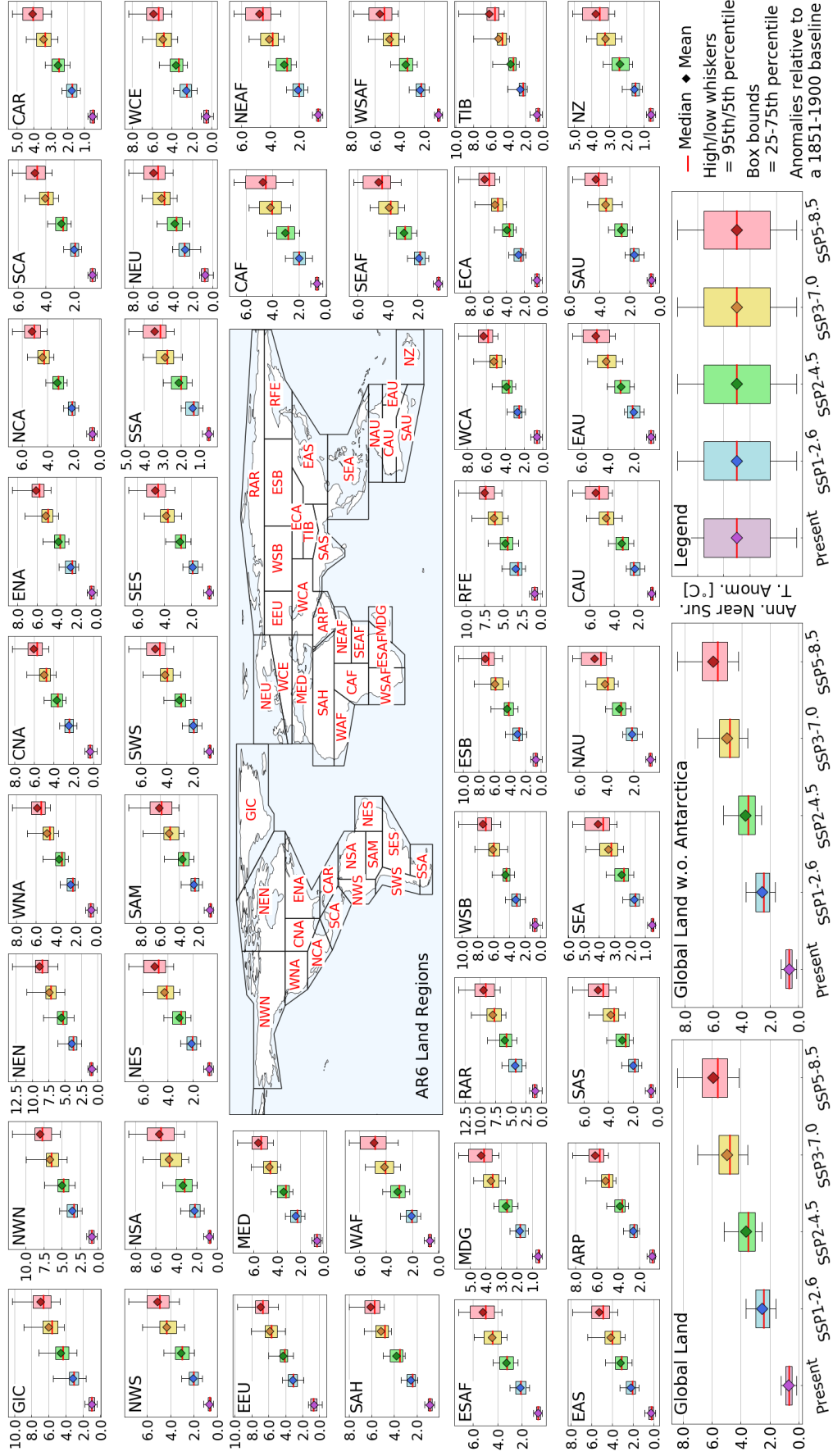


Figure 3: Multi-model ensemble projections of change in the average annual near surface temperature from the pre-industrial (1851-1900) to the present day (1981-2010), and four future scenarios (2071-2100). Only land grid values of a region are considered when averaging.

Spatial projections of multi-model ensemble average annual number of tropical nights ($TR_{\bar{A}}$) for the present day, SSP1-2.6, SSP2-4.5, SSP3-7.0, and SSP5-8.5, along with the corresponding change from a pre-industrial baseline and inter-model variability, are presented in Figure 4. As annual average temperature, broad patterns are visible across projections. For example, $TR_{\bar{A}}$ is greatest across equatorial regions, and least amongst polar and high-altitude regions. Another pattern is apparent in the pre-industrial anomalies, namely that the largest deviations of a given scenario are projected for northwestern and western South America, and sub-Saharan Africa. It is worth noting that the magnitude of increase in $TR_{\bar{A}}$, both absolute and relative to the pre-industrial, increases with increasing GHG concentrations. For instance, under SSP1-2.6, northern mid-latitudes are projected to endure 1-20 tropical nights, whereas under SSP5-8.5, this increases to 10-50. Similarly, the Tibetan Plateau region where $TR_{\bar{A}} = 0$ contracts as GHG concentrations increase. Furthermore, the northern mid-latitudes and equatorial regions show contrasting inter-model variability behaviour with increasing GHG concentrations, with the former exhibiting greatest variability under the present day, and the latter under SSP5-8.5. This is likely due to the threshold nature of $TR_{\bar{A}}$. Variability will be greatest when daily minimum NST is close to the 20°C threshold as, for example, even if a region has a temperature range of 25-40°C, the $TR_{\bar{A}}$ variability would be low as this range lies above the threshold.

A regional analysis of changes in $TR_{\bar{A}}$ from pre-industrial levels is presented in Figure 5. Globally, excluding Antarctica, $TR_{\bar{A}}$ is projected to increase by 10.6, 30.3, 43.7, 57.7, and 66.9 days from the pre-industrial for the present day, SSP1-2.6, SSP2-4.5, SSP3-7.0, and SSP5-8.5 respectively. Moreover, the end of the twenty-first century change from the pre-industrial is greatest under SSP5-8.5, and least under SSP1-2.6 for all 44 regions. Additionally, SEAF (southern East Africa) ranks first within each future scenario for greatest absolute pre-industrial increase in $TR_{\bar{A}}$, with neighbouring regions of CAF (central Africa), ESAF (east southern Africa), and WSAF (west southern Africa) often sharing the second and third ranks. Naturally, in absolute terms, smallest increases are for regions where historically a TR is rare, such as GIC (Greenland and Iceland). In addition, the number of regions where $TR_{\bar{A}} > 300$ days is 3, 5, 9, and 10 under SSP1-2.6, SSP2-4.5, SSP3-7.0, and SSP5-8.5 respectively, and so SSP1-2.6 has less regions with dangerously high $TR_{\bar{A}}$. It is important to note that for regions projected to experience almost daily tropical nights, such as CAR (Caribbean), the rate of increase in $TR_{\bar{A}}$ appears to halt with increasing GHG concentrations, yet this is because $TR_{\bar{A}}$ is already at its maximum. Subsequently, this is not evidence that, after a certain threshold, increasing GHGs do not contribute to increasing $TR_{\bar{A}}$. Lastly, variability across model members is greatest under high GHG concentrations, and a positive skew is apparent. In short, $TR_{\bar{A}}$ is projected to increase regardless of scenario, yet is avoided most under SSP1-2.6.

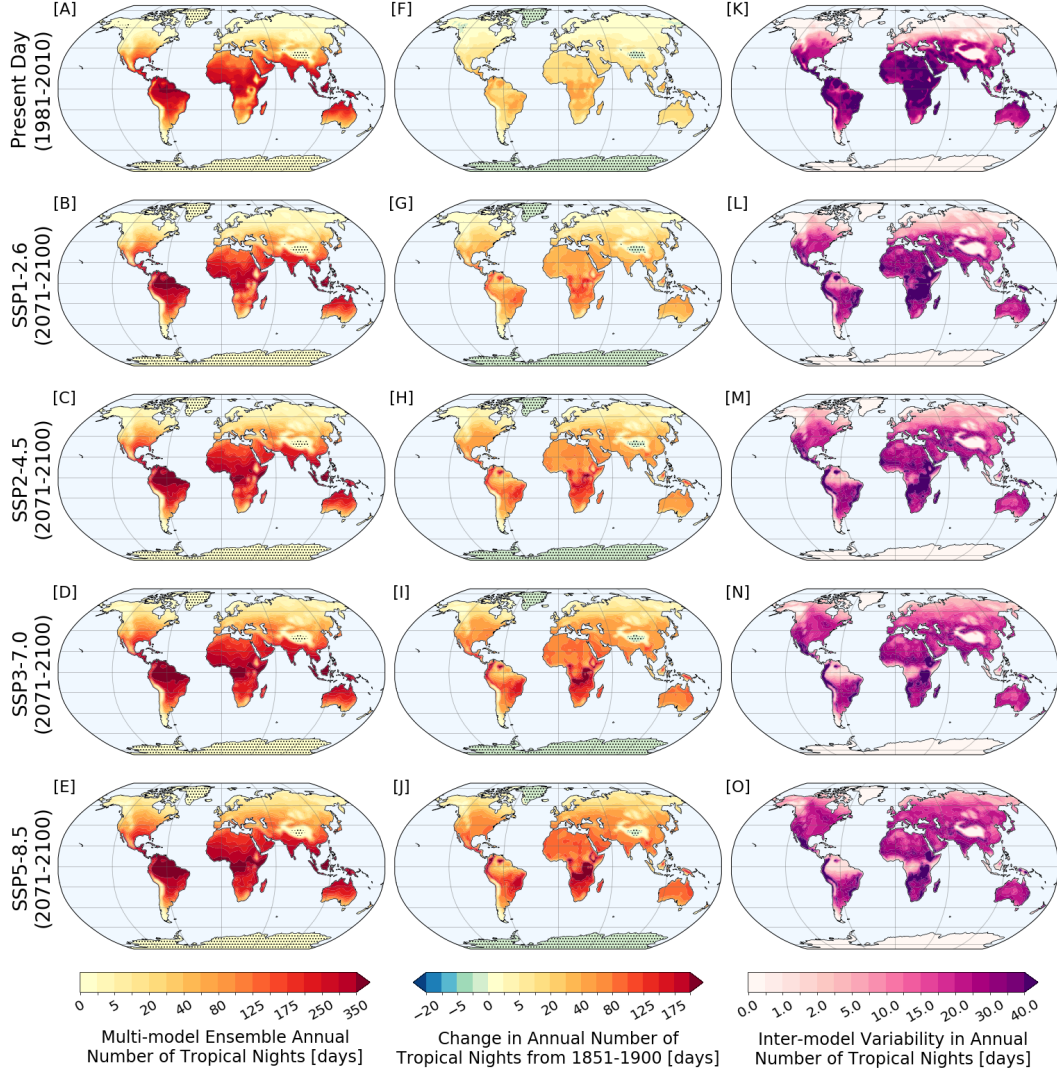


Figure 4: [A-E] Multi-model ensemble projections of average annual number of tropical nights, [F-J] the associated change from a pre-industrial baseline (1851-1900), [K-O] and the inter-model variability for the present day (1981-2010), and four future scenarios (2071-2100). Ocean areas are masked for clarity. Dotted regions represent zero values.

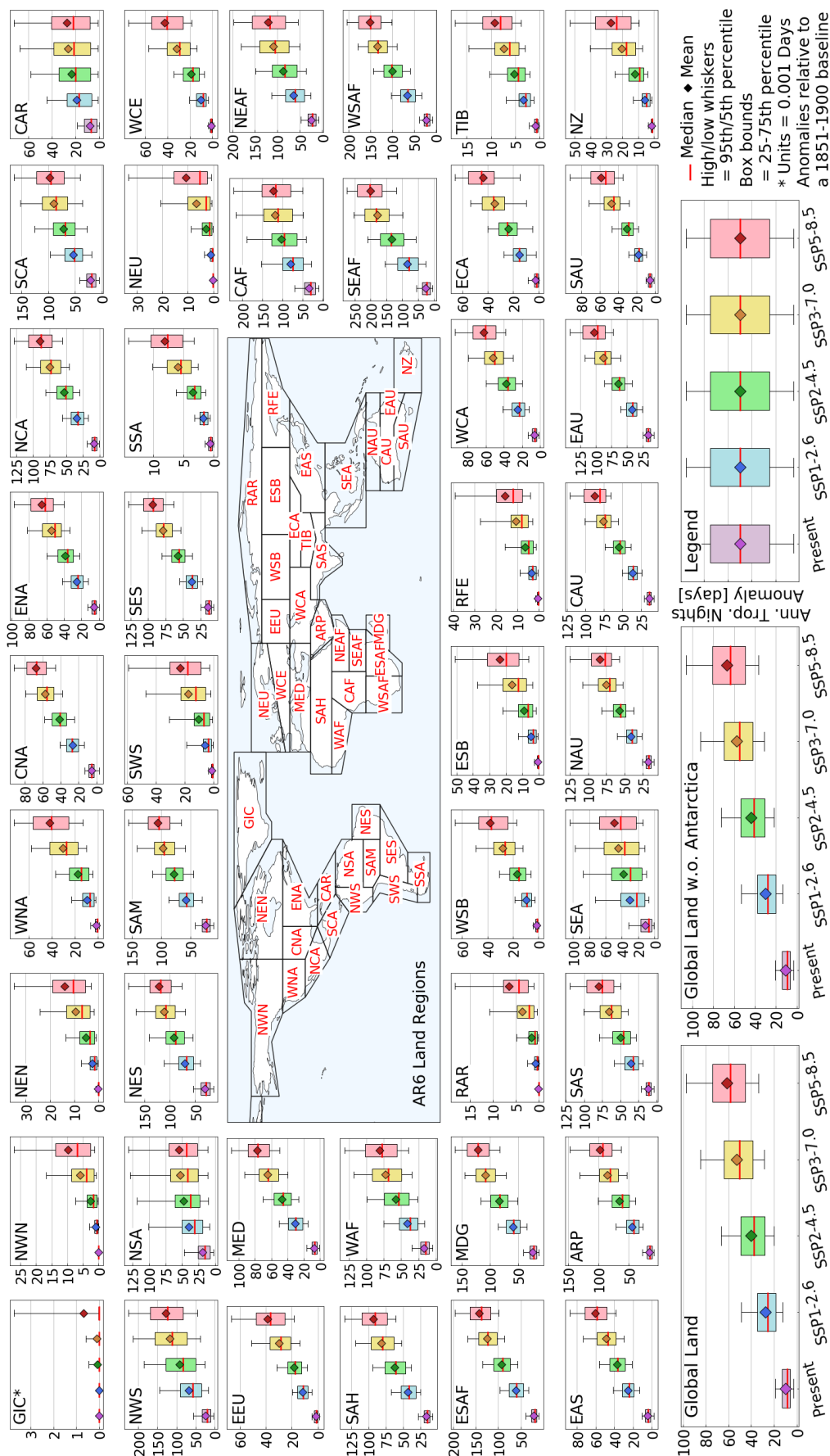


Figure 5: Multi-model ensemble projections of change in the average annual number of tropical nights from the pre-industrial to the present day (1981-2010), and four future scenarios (2071-2100). Only land grid cell values of a region are considered when averaging.

3.3 Population and Heat Exposure

The global population is projected to rise from the pre-industrial with increases compared to the pre-industrial baseline of 301.0%, 438.2%, 555.1%, 740.2%, and 463.3% projected for the present day, SSP1, SSP2, SSP3, and SSP5 respectively. Unsurprisingly, the most populated region for the present day is EAS (eastern Asia) and SAS (southern Asia) which, combined, hold 42.3% of the global population. Whereas regions least populated are naturally those with harsh environments such as CAU (central Australia) and GIC. These geographic patterns extend into future projections, yet there is clear variation between different pathways. For example, under SSP3, low population growth in high income countries sees minor population increases from the present day in North America, and decreases in Europe, with some areas of the latter showing decreases from the pre-industrial. Conversely, the same high income countries under SSP5 experience high population growth, the greatest seen in WNA (western North America), CNA (central North America), and NEU (northern Europe) where growth exceeding 100% is projected. Similarly, variation between SSP3 and SSP5 is evident for high fertility countries. For instance, under SSP3, high population growth in WAF (western Africa) and SAS sees populations 3384.9% and 891.8% greater than the pre-industrial respectively. Whereas under the low growth of SSP5, these values reduce to 1705.5% and 433.4% accordingly. Lastly, it is worth noting that population loss from the present day is projected for EEU (eastern Europe) and EAS regardless of the future pathway followed. In summary, global future population increases are avoided most under SSP1 and SSP5, yet this is not consistent regionally, as developing and developed countries exhibit varying behaviour for a given pathway.

Present day and end of the twenty-first century multi-model ensemble projections of average annual exposure to tropical nights, $H_{\bar{A}}$, along with the corresponding change from a pre-industrial baseline and inter-model variability, are presented in Figure 6. Clear patterns are evident across the projections with $H_{\bar{A}}$, and its change from the pre-industrial, greatest for equatorial regions and the Indian subcontinent, and least, excluding uninhabited areas, across northern mid-latitudes, southern South America, and some areas within the Tibetan Plateau. The decrease in $H_{\bar{A}}$ from the pre-industrial seen in Australia is likely a methodology discrepancy between the two different underlying population projections used as opposed to a true reduction in exposure. Furthermore, as population projections without upper and lower estimates are used, the variability of $H_{\bar{A}}$ results entirely from the climate model outputs. Nevertheless, the pattern will differ to that of $TR_{\bar{A}}$ as the population present will amplify the variability of some areas more than others. In addition, $H_{\bar{A}}$ is displayed alongside $TR_{\bar{A}}$ and population projections in Figure 7, making the underlying relationship apparent. For example, northeastern South America has substantially greater $TR_{\bar{A}}$ than western Europe. However, due to the former's relatively low population, $H_{\bar{A}}$ is in fact lower in northeastern South America. Similarly, the high population of the Indian subcontinent causes this area to have the greatest $H_{\bar{A}}$ despite lower $TR_{\bar{A}}$ values than equatorial regions.

Regional and global aggregated changes in $H_{\bar{A}}$ from the pre-industrial are displayed in Figure 8. Presently, the $H_{\bar{A}}$ pre-industrial anomaly is 620 billion person-days, whereas by the end of the twenty-first century this deviation increases to 1192, 1684, 2527, and 1544 billion person-days under SSP1-2.6, SSP2-4.5, SSP3-7.0, and SSP5-8.5 respectively. As well as having the greatest global exposure projection, SSP3-7.0 shows the greatest variability in exposure across ensemble members, followed by SSP2-4.5, and then SSP1-2.6 and SSP5-8.5. However, these global scale patterns are not consistent for all regions. For instance, of the 44 regions, $H_{\bar{A}}$ projections are greatest under SSP3-7.0 for 30 regions, with the remainder greatest under SSP5-8.5. These 30 regions following global scale trends are mainly developing regions from sub-Saharan Africa, whereas those deviating are largely mid-latitude developed regions such as NZ, EAU (eastern Australia), WCE (western central Europe), and ENA (eastern North America). Likewise, the pathway which minimises

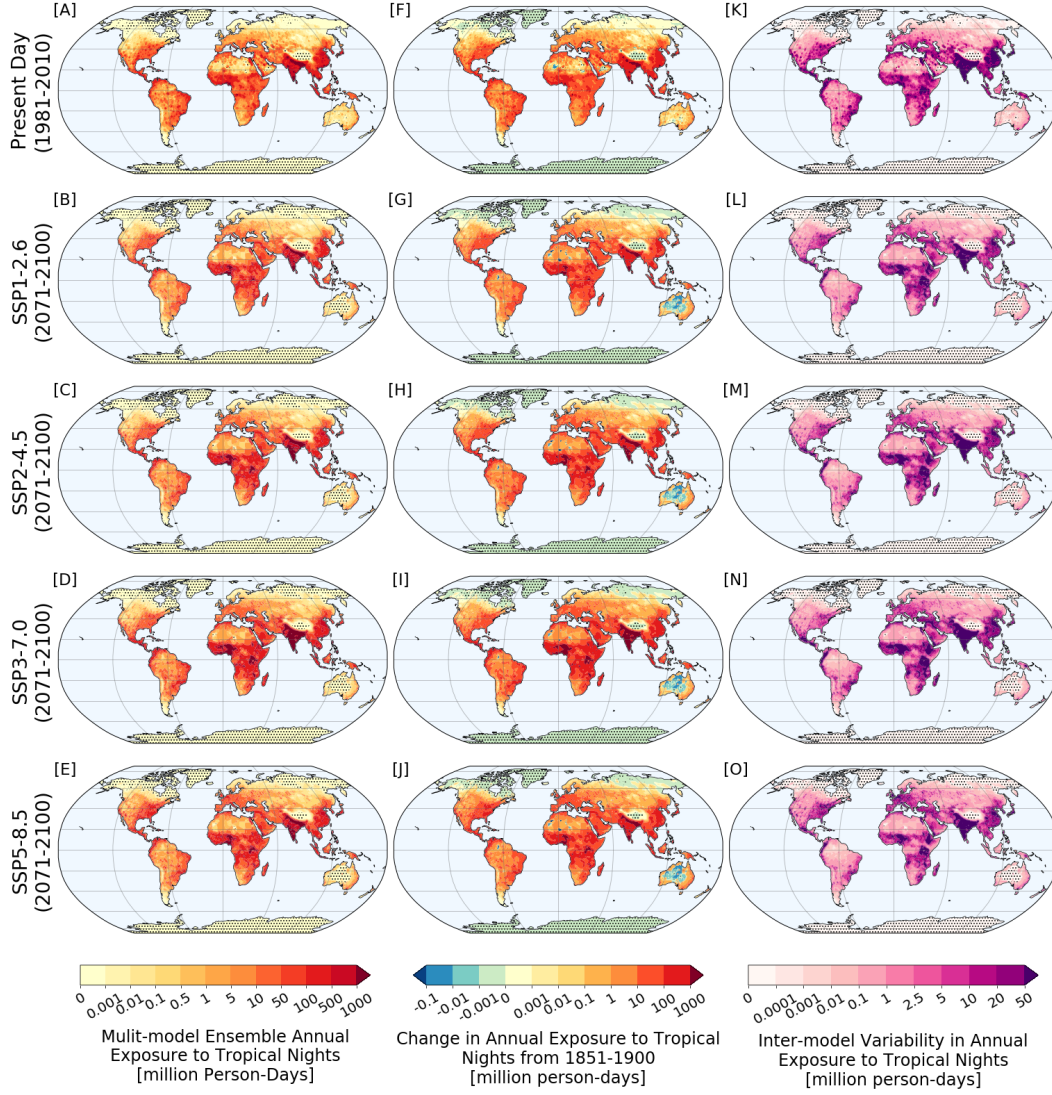


Figure 6: [A-E] Multi-model ensemble projections of average annual exposure to tropical nights, [F-J] the associated change from a pre-industrial baseline (1851-1900), [K-O] and the inter-model variability for the present day (1981-2010), and four future scenarios (2071-2100). Ocean areas are masked for clarity. Dotted regions represent zero values.

future $H_{\bar{A}}$ most varies across regions. For example, under SSP1-2.6, $H_{\bar{A}}$ is lowest for 39 regions, of which both EAS and SSA exhibit a reduction in exposure from the present day. Of the remaining regions, $H_{\bar{A}}$ is lowest for EAU, CAU, CNA, and ENA (eastern North America) under SSP3-7.0, and for CAR under SSP5-8.5 which, surprisingly, projects a 12.5% decrease in $H_{\bar{A}}$ from the present day despite considerably higher GHG concentrations. In short, under SSP1-2.6 the increase in future exposure is minimised, whereas its increase is greatest under SSP3-7.0 and SSP5-8.5 for developing and developed regions respectively, yet exceptions do exist.

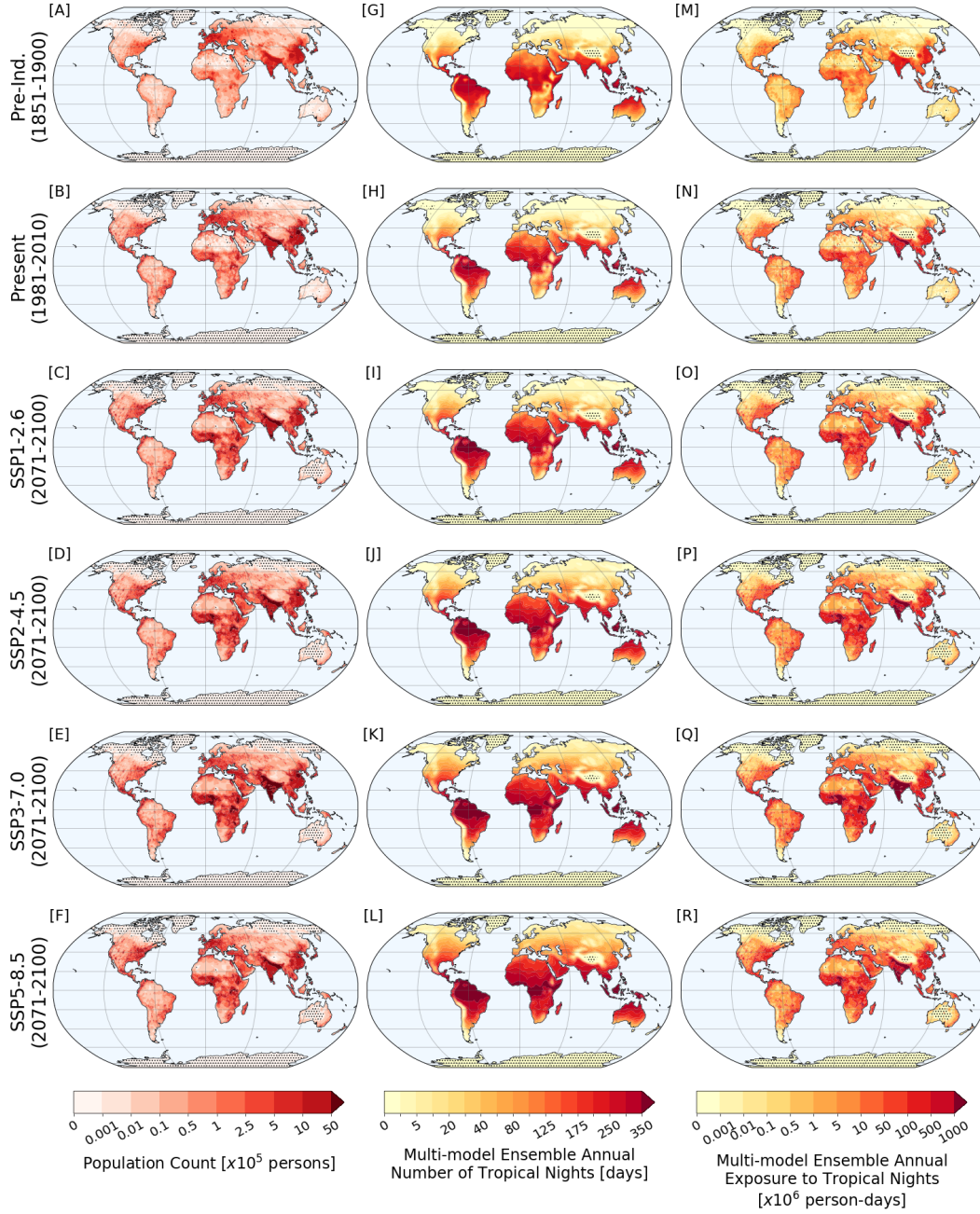
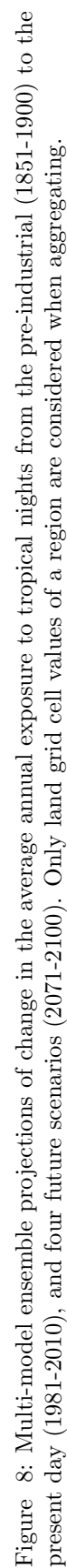


Figure 7: A combination view of [A-F] projected total population distributions, [G-L] multi-model ensemble projections of average annual number of tropical nights, [M-R] and multi-model ensemble projections of average annual exposure to tropical nights for the pre-industrial (1851-1900), present day (1981-2010), and four future scenarios (2071-2100). Ocean areas are masked for clarity. Dotted regions represent zero values.



4 Discussion

This study has used GCM and ESM simulations contributing to CMIP6 to project future change in the number of tropical nights occurring annually relative to a pre-industrial baseline. Although currently no studies of the same nature exist, comparison with those using previous CMIP5 simulations can be made as both contain scenarios using the same levels of radiative forcing. For example, future global and regional increase in the frequency of tropical nights with increasing radiative forcing is a correlation which features in both this study and similar studies using CMIP5 model simulations (e.g. Orłowsky and Seneviratne (2012); IPCC (2013); Sillmann, Kharin, Zwiers, et al. (2013)). Indeed, this correlation is also found in observational data (Morak et al., 2011) and historical simulations (Sillmann, Kharin, Zhang, et al., 2013). Hence, this suggests, perhaps unsurprisingly, that minimising the change in the frequency of tropical nights from the pre-industrial is best achieved following pathways describing low radiative forcing futures, such as SSP1-2.6. As an illustration, by following SSP1-2.6 over SSP5-8.5, an additional 36.6 tropical nights annually can be avoided at the global scale by the end of the twenty-first century which equates to a reduction of 22.3%. Regionally this percentage reduction between SSP5-8.5 and SSP3-7.0 varies substantially, between 2.4-89.1%, with values smallest for equatorial regions and increasing as regions approach the poles, especially those of the Northern Hemisphere. As a result, in terms of avoiding increasing tropical nights frequency, some communities will benefit more under SSP1-2.6 than others, and so likely advocate worldwide adoption of the socioeconomic values described by this pathway to a greater extent. This could potentially aggravate existing divisions within environmental politics (Tranter, 2011; McCright et al., 2016). Moreover, these communities where increases can be avoided most are found in southern and southeastern Africa where the avoidance of up to 115 tropical nights annually is possible. However, as mentioned previously, the alarming scarcity of extreme heat studies focusing on these regions may cause such potential to go unrecognised by policy makers. In contrast, studies of northern mid-latitudes are widely available facilitating greater comparison with the findings of this study. For example, under SSP5-8.5, this study projects the annual number of tropical nights to be 10-20 days greater than those simulated by CMIP5 models for the same level of radiative forcing (Viceto et al., 2019; Cardoso et al., 2019). Likewise, this deviation, albeit of smaller magnitude, is also present in other heavily studied areas, such as eastern Australia and western North America under these high radiative forcing scenarios (Sillmann, Kharin, Zwiers, et al., 2013). Whereas, the CMIP6 and CMIP5 simulations are more aligned when driven by lower radiative forcing. Consequently, this study finds that projected reductions in tropical nights frequency for these regions tend to be higher than those of CMIP5. However, due to slightly differing regional boundaries employed between CMIPs, the robustness of this trend warrants further work. Lastly, it is important to note that under no scenario are annual tropical nights projected to reduce from either pre-industrial or present day levels. Hence, industries, infrastructure, ecosystems, and other areas sensitive to nightly high temperatures, should be evaluated and, if required, prepared to handle these future increases.

By coupling population distribution projections with climate simulations from CMIP6 models, this study is able to project future annual human exposure to tropical nights relative to a pre-industrial baseline. Globally the rise in future exposure from pre-industrial levels is minimised under SSP1-2.6, which, when compared to SSP3-7.0, avoids 1336 billion person-days. In contrast with tropical nights, the pathway which avoids future exposure most varies region by region, as has been found in previous studies, albeit of different heat events (Jones et al., 2018; Arnell et al., 2019; Wang et al., 2020). This variation is clear evidence that changes in population does influence exposure. This is because, if exposure was only dependent on changes in climate, all regional exposure would be minimised under SSP1-2.6 as this is the pathway which minimises an increase in tropical night frequency. Moreover, the relative influence of climate and population changes differs across regions. For example, in the Caribbean and northern South America, as

tropical nights are projected almost daily under all future pathways, future exposure is primarily influenced by changes in population. In contrast, for regions where population changes are fairly constant by the end of the twenty-first century, such as central Australia, projected exposure is predominantly influenced by climatic changes. Similarly, despite future tropical night frequency increasing across eastern Asia and southern South America, under SSP1-2.6 exposure is projected to reduce from the present day, evidently suggesting that the influence of population change is greater than that of climate for this pathway. Such patterns in influence are reported for other heat events, albeit more quantitatively, in other studies (Z. Liu et al., 2017; Jones et al., 2018). Furthermore, this work finds that for developed and developing countries the greatest exposure is projected under SSP5-8.5 and SSP3-7.0 respectively. As developed countries historically have more global influence, this divide could lead to the promotion of pathways not necessarily in the best interest of developing countries. In addition, unsurprisingly, densely populated regions lying close to the equator such as the Indian subcontinent, western Africa, and southeastern Asia, have the highest change in exposure from the pre-industrial in absolute terms. However, these areas also have the greatest reduction potential suggesting these should be treated as key regions in global efforts to avoid future exposure. Lastly, it is important to note that, although under SSP1-2.6 overall future exposure is avoided most, there still exists regions with substantial exposure to tropical nights in this scenario. This suggests that, for select regions, high levels of exposure will be inevitable. As such, it is imperative that adaptive measures are implemented for these areas.

One main caveat to this work is the use of population projections from two different sources, and subsequently differing methodologies, to analyse population change. In this study, pre-industrial and present day distributions are derived from HYDE 3.2, whereas those of the end of the twenty-first century are from projections by NCAR-CDIR. Consequently, this introduces added uncertainty to this study's analysis as it is unclear as to whether deviations from the pre-industrial are true projected changes, or whether they arise due to the differing underlying methodologies. Nevertheless, the use of both sources was a necessity to enable this study's end of the twenty-first century comparison with the pre-industrial as currently there exist no suitable population projections which cover this temporal range entirely. As such, a future effort to enhance the temporal coverage of population projections will be of great use to similar studies to follow. Furthermore, population projections are incorporated into this work without uncertainty ranges meaning variation in exposure to tropical nights arises solely from the climate ensemble members which limits the confidence in the uncertainty ranges of exposure quoted in this study. Future works should use population projections which include likely value ranges to avoid similar limitations. Lastly, the population projections used do not account for intra-annual migration and so the fact that a region's population is a dynamic variable in perpetual fluctuation is not accounted for. For example, if a region's population is below the annual average when tropical nights are likely to occur, the true annual exposure is less than what this study quotes. It would be of interest to compare a future study focusing on seasonal exposure to tropical nights to see how seasonal population variation impacts the values quoted here.

At the time of this study, the required variables, monthly and daily minimum temperatures, have only been simulated by 15 CMIP6 models under the necessary runs. Subsequently, the multi-model ensemble used in this work is not fully populated meaning the full uncertainty in climate outcomes may not have been explored adding uncertainty to the findings derived. Nevertheless, this added uncertainty remains low relative to similar studies which use single model output to derive their respective extreme event indices meaning an improvement has been made. This improvement is evident in the greater performance of the multi-model ensemble relative to its individual members. Furthermore, three pairs of models sharing the same atmospheric component are found to exhibit strikingly similar spatial performance. This suggests a violation of the model independence assumption used in this study. Moreover, the performance of coarser reso-

lution models is found to be greater than those of finer resolutions when simulating the annual number of tropical nights. Consequently, it could benefit future works to deviate from this study's equal weighting of ensemble members in order to adjust for these behaviours. Although, as conclusions of model performance may differ with alternative measures of performance and observation datasets, future work should ensure these behaviours are robust before accounting for them.

This work does not account for urban areas often being warmer than surrounding rural areas due to the added heat generated from the increase in human activity, a phenomenon known as the urban heat island effect (Oke, 1982). Studies have noted that the difference between urban and rural areas can be as much as 2-3°C (Stewart & Oke, 2012), and this range is found to be even larger during a heat event (Li & Bou-Zeid, 2013). As this study does not attempt to account for these temperature differences, such as using climate simulations producing separate urban and rural outcomes, the urban heat island effect is not represented. Hence, it is possible this work underestimates the number of tropical nights experienced by urban populations. This underestimation will be greatest under scenarios with greater levels of urbanisation, such as SSP1-2.6 and SSP5-8.5, as opposed to those where future urban areas are less populated. This will effectively reduce the exposure range seen across the future pathways as the lower bound, largely under SSP1-2.6, will rise. Consequently, global and regional estimations of avoided exposure made in this study are likely greater than their true values, yet, judging from the magnitude of this difference found in other studies (Z. Liu et al., 2017; Jones et al., 2018), not accounting for the urban heat island effect should not impact on this study's main conclusions on which pathways avoid greatest change.

5 Conclusions

This study is among initial research beginning to explore CMIP6 model simulations in the context of exposure to extreme heat events. Projections of annual exposure to tropical nights for the pre-industrial, present day, and four futures described by SSP1-2.6, SSP2-4.5, SSP3-7.0, and SSP5-8.5, have been presented. These have been supplemented with similar projections of tropical night frequency, total population, and near surface temperature. A deliberate focus has been made to quantify future change relative to the pre-industrial such that pathways which minimise detrimental change can be highlighted. This study finds that global annual exposure to tropical nights is projected to increase from pre-industrial levels by 814-1055% by the end of the twenty-first century depending on the pathway followed. Similarly, both underlying determinants of this exposure are projected to increase substantially from the pre-industrial with the global average annual number of tropical nights and total population projected to increase by 32-71% and 438-740% respectively across the four alternative futures. Importantly, this study finds that these global increases can be mitigated by adopting the socioeconomic values central to the SSP1-2.6 narrative, yet under no scenario do they become decreases. This finding largely holds at the regional scale in terms of exposure, although there are notable exceptions. Overall, this study acts as a first assessment of how tropical nights and humanity's exposure to them is set to change as this century progresses. This work looks to encourage subsequent studies to provide more insights into the results that have been discussed here. With tropical nights already impeding on humanity, the projected increases that have been highlighted must act as an incentive to develop mitigation and adaptive measures for the benefit of all, otherwise undesirable consequences loom.

Acknowledgments

All data from CMIP6 simulations used in our analyses are freely available from the Earth System Grid Federation (<https://esgf-node.llnl.gov/search/cmip6/>). We would like to thank all the CMIP6 modelling groups for creating and providing this data. This work used JASMIN, the UK's collaborative data analysis environment (<http://jasmin.ac.uk>).

HadCRUT data are freely available from the Hadobs website (<https://www.metoffice.gov.uk/hadobs/hadex2/>). The underlying code used in this study is made available at: <https://github.com/mscprojectusername/msc-dissertation.git>.

References

- Alexander, L., Zhang, X., Peterson, T., Caesar, J., Gleason, B., et al. (2006). Global observed changes in daily climate extremes of temperature and precipitation. *Journal of Geophysical Research - Atmospheres*, 111(D05109).
- Amengual, A., Homar, V., Romero, R., Brooks, H., Ramis, C., et al. (2014). Projections of heat waves with high impact on human health in Europe. *Global and Planetary Change*, 119, 71-84.
- Arnell, N., Lowe, J., Bernie, D., Nicholls, R., Brown, S., et al. (2019). The global and regional impacts of climate change under representative concentration pathway forcings and shared socioeconomic pathway socioeconomic scenarios. *Environmental Research Letters*, 14(084046).
- Barriopedro, D., Fischer, E., Luterbacher, J., Trigo, R., & Garcia-Herrera, R. (2011). The hot summer of 2010: Redrawing the temperature record map of Europe. *Science*, 332, 220-224.
- Boucher, O., Servonnat, J., Albright, A., Aumont, O., Balkanski, Y., et al. (2020). Presentation and evaluation of the IPSL-CM6A-LR climate model. *Journal of Advances in Modeling Earth Systems*, 12(e2019MS002010).
- Boudet, H., Giordano, L., Zanocco, C., Satein, H., & Whitley, H. (2020). Event attribution and partisanship shape local discussion of climate change after extreme weather. *Nature Climate Change*, 10, 69-76.
- Cardoso, R., Soares, P., Lima, D., & Miranda, P. (2019). Mean and extreme temperatures in a warming climate: EURO CORDEX and WRF regional climate high-resolution projections for Portugal. *Climate Dynamics*, 52, 129-157.
- Carleton, T., & Hsiang, S. (2016). Social and economic impacts of climate. *Science*, 353(aad9837).
- Ceccherini, G., Russo, S., Amezttoy, I., Marchese, A., & Carmona-Moreno, C. (2017). Heat waves in Africa 1981-2015, observations and reanalysis. *Natural Hazards and Earth System Sciences*, 17, 115-125.
- Ceccherini, G., Russo, S., Amezttoy, I., Romero, C., & Carmona-Moreno, C. (2016). Magnitude and frequency of heat and cold waves in recent decades: The case of South America. *Natural Hazards and Earth System Sciences*, 16, 821-831.
- Coumou, D., & Robinson, A. (2013). Historic and future increase in the global land area affected by monthly heat extremes. *Environmental Research Letters*, 8(034018).
- Cowan, T., Purich, A., Perkins, S., Pezza, A., Bosch, G., et al. (2014). More frequent, longer, and hotter heat waves for Australia in the twenty-first century. *Journal of Climate*, 27, 5851-5871.
- DeGaetano, A., & Allen, R. (2002). Trends in twentieth-century temperature extremes across the United States. *Journal of Climate*, 15, 3188-3205.
- Donat, M., Alexander, L., Yang, H., Durre, I., Vose, R., et al. (2013). Updated analyses of temperature and precipitation extreme indices since the beginning of the twentieth century: The HadEX2 dataset. *Journal of Geophysical Research - Atmospheres*, 118, 2098-2118.
- Donat, M., Peterson, T., Brunet, M., King, A., Almazroui, M., et al. (2014). Changes in extreme temperature and precipitation in the Arab region: Long-term trends and variability related to ENSO and NAO. *International Journal of Climatology*, 34, 581-592.
- Dosio, A., Mentaschi, L., Fischer, E., & Wyser, K. (2018). Extreme heat waves under 1.5 degrees c and 2 degrees c global warming. *Environmental Research Letters*, 13(054006).

- Dottori, F., Szewczyk, W., Ciscar, J., Zhao, F., Alfieri, L., et al. (2018). Increased human and economic losses from river flooding with anthropogenic warming. *Nature Climate Change*, 8, 781-786.
- Dunne, J., Horowitz, L., Adcroft, A., Ginoux, P., Held, I., et al. (2020). The GFDL Earth System Model version 4.1 (GFDL-ESM4.1): Overall coupled model description and simulation characteristics. *Journal of Advances in Modelling Earth Systems*, 12(e2019MS002015).
- Eyring, V., Bony, S., Meehl, G., Senior, C., Stevens, B., et al. (2016). Overview of the Coupled Model Intercomparison Project Phase 6 (CMIP6) experimental design and organization. *Geoscientific Model Development*, 9, 1937-1958.
- Feron, S., Cordero, R., Damiani, A., Llanillo, P., Jorquera, J., et al. (2019). Observations and projections of heat waves in South America. *Scientific Reports*, 9(8173).
- Ferranti, E., Chapman, L., Lee, S., Jaroszweski, D., Lowe, C., et al. (2018). The hottest July day on the railway network: Insights and thoughts for the future. *Meteorological Applications*, 25, 195-208.
- Fischer, E., & Knutti, R. (2015). Anthropogenic contribution to global occurrence of heavy-precipitation and high-temperature extremes. *Nature Climate Change*, 5, 560-564.
- Fontaine, B., Janicot, S., & Monerie, P. (2013). Recent changes in air temperature, heat waves occurrences, and atmospheric circulation in Northern Africa. *Journal of Geophysical Research - Atmospheres*, 118, 8536-8552.
- Founda, D., Varotsos, K., Pierros, F., & Giannakopoulos, C. (2019). Observed and projected shifts in hot extremes' season in the Eastern Mediterranean. *Global and Planetary Change*, 175, 190-200.
- Frei, C., & Schar, C. (2001). Detection probability of trends in rare events: Theory and application to heavy precipitation in the Alpine region. *Journal of Climate*, 14, 1568-1584.
- Gleckler, P., Taylor, K., & Doutriaux, C. (2008). Performance metrics for climate models. *Journal of Geophysical Research - Atmospheres*, 113(D06104).
- Goldewijk, K., Beusen, A., & Janssen, P. (2010). Long-term dynamic modeling of global population and built-up area in a spatially explicit way: HYDE 3.1. *Holocene*, 4, 565-573.
- Herring, S., Christidis, N., Hoell, A., Hoerling, M., & P.A., S. (2020). Explaining extreme events of 2018 from a climate perspective. *Bulletin of the American Meteorological Society*, 101, S1-S128.
- Herring, S., Christidis, N., Hoell, A., Hoerling, M., & Stott, P. (2019). Explaining extreme events of 2017 from a climate perspective. *Bulletin of the American Meteorological Society*, 100, S1-S117.
- Herring, S., Christidis, N., Hoell, A., Kossin, J., Schreck, C., et al. (2018). Explaining extreme events of 2016 from a climate perspective. *Bulletin of the American Meteorological Society*, 99, S1-S157.
- Herring, S., Hoell, A., Hoerling, M., Kossin, J., Schreck, C., et al. (2016). Explaining extreme events of 2015 from a climate perspective. *Bulletin of the American Meteorological Society*, 97, S1-S145.
- Herring, S., Hoerling, M., Kossin, J., Peterson, T., & Stott, P. (2015). Explaining extreme events of 2014 from a climate perspective. *Bulletin of the American Meteorological Society*, 96, S1-S172.
- Hopke, J. (2020). Connecting extreme heat events to climate change: Media coverage of heat waves and wildfires. *Environmental Communication*, 14, 492-508.
- Horton, R., Mankin, J., Lesk, C., Coffel, E., & Raymond, C. (2016). A review of recent advances in research on extreme heat events. *Current Climate Change Reports*, 2, 242-259.
- IPCC. (2013). *Climate Change 2013: The Physical Science Basis. Contribution of Working Group I to the Fifth Assessment Report of the Intergovernmental*

- Panel on Climate Change [Book]. Cambridge, United Kingdom and New York, NY, USA: Cambridge University Press.
- Iturbide, M., Gutiérrez, J. M., Alves, L. M., Bedia, J., Cerezo-Mota, R., Gimenez, E., ... Vera, C. S. (2020). An update of ipcc climate reference regions for subcontinental analysis of climate model data: definition and aggregated datasets. *Earth System Science Data*, 12(4), 2959–2970. doi: 10.5194/essd-12-2959-2020
- Jones, B., & O'Neill, B. (2013). Historically grounded spatial population projections for the continental United States. *Environmental Research Letters*, 8(044021).
- Jones, B., & O'Neill, B. (2016). Spatially explicit global population scenarios consistent with the Shared Socioeconomic Pathways. *Environmental Research Letters*, 11(084003).
- Jones, B., Tebaldi, C., O'Neill, B., Oleson, K., & Gao, J. (2018). Avoiding population exposure to heat-related extremes: Demographic change vs climate change. *Climatic Change*, 146, 423–437.
- Karl, T., & Easterling, D. (1999). Climate extremes: Selected review and future research directions. *Climatic Change*, 42, 309–325.
- Knutti, R., Furrer, R., Tebaldi, C., Cermak, J., & Meehl, G. (2007). Challenges in combining projections from multiple climate models. *Journal of Climate*, 23, 2739–2758.
- Law, R., Ziehn, T., Matear, R., Lenton, A., Chamberlain, M., et al. (2017). The carbon cycle in the Australian Community Climate and Earth System Simulator (ACCESS-ESM1) - Part 1: Model description and pre-industrial simulation. *Geoscientific Model Development*, 10, 2567–2590.
- Lee, J., Hong, S., Chang, E., Suh, M., & Kang, H. (2014). Assessment of future climate change over East Asia due to the RCP scenarios downscaled by GRIMs-RMP. *Climate Dynamics*, 42, 733–747.
- Lelieveld, J., Hadjinicolaou, P., Kostopoulou, E., Giannakopoulos, C., Pozzer, A., et al. (2014). Model projected heat extremes and air pollution in the eastern Mediterranean and Middle East in the twenty-first century. *Regional Environmental Change*, 14, 1937–1949.
- Li, D., & Bou-Zeid, E. (2013). Synergistic interactions between urban heat islands and heat waves: The impact in cities is larger than the sum of its parts. *Journal of Applied Meteorology and Climatology*, 52, 2051–2064.
- Liu, W., Sun, F., Lim, W., Zhang, J., Wang, H., et al. (2018). Global drought and severe drought-affected populations in 1.5 and 2 degrees c warmer worlds. *Earth System Dynamics*, 9, 267–283.
- Liu, Z., Anderson, B., Yan, K., Dong, W., Liao, H., & Shi, P. (2017). Global and regional changes in exposure to extreme heat and the relative contributions of climate and population change. *Scientific Reports*, 7.
- Luo, M., & Lau, N. (2017). Heat waves in southern China: Synoptic behavior, long-term change, and urbanization effects. *Journal of Climate*, 30, 703–720.
- Luo, M., Ning, G., Xu, F., Wang, S., Liu, Z., et al. (2020). Observed heatwave changes in arid northwest China: Physical mechanism and long-term trend. *Atmospheric Research*, 242(UNSP:105009).
- McCright, A., Dunlap, R., & Marquart-Pyatt, S. (2016). Political ideology and views about climate change in the European Union. *Environmental Politics*, 25, 338–358.
- Mearns, L., Katz, R., & Schneider, S. (1984). Extreme high temperature events - Changes in their probabilities with changes in mean temperature. *Journal of Climate and Applied Meteorology*, 23, 1601–1613.
- Meehl, G., Covey, C., Delworth, T., Latif, M., McAvaney, B., et al. (2007). The WCRP CMIP3 multimodel dataset - A new era in climate change research. *Bulletin of the American Meteorological Society*, 88, 1383–1394.
- Meehl, G., Covey, C., McAvaney, B., Latif, M., & Stouffer, R. (2005). Overview of

- the Coupled Model Intercomparison Project. *Bulletin of the American Meteorological Society*, 86, 89-93.
- Mishra, V., Ganguly, A., Nijssen, B., & Lettenmaier, D. (2015). Changes in observed climate extremes in global urban areas. *Environmental Research Letters*, 10(024005).
- Morak, S., Hegerl, G., & Kenyon, J. (2011). Detectable regional changes in the number of warm nights. *Geophysical Research Letters*, 38(L17703).
- Moron, V., Oueslati, B., Pohl, B., Rome, S., & Janicot, S. (2016). Trends of mean temperatures and warm extremes in northern tropical Africa (1961-2014) from observed and PPCA-reconstructed time series. *Journal of Geophysical Research - Atmospheres*, 121, 5298-5319.
- Muller, W., Jungclaus, J., Mauritsen, T., Baehr, J., Bittner, M., et al. (2018). A higher-resolution version of the Max Planck Institute Earth System Model (MPI-ESM1.2-HR). *Journal of Advances in Modeling Earth Systems*, 10, 1383-1413.
- Murari, K., Ghosh, S., Patwardhan, A., Daly, E., & Salvi, K. (2014). Intensification of future severe heat waves in India and their effect on heat stress and mortality. *Regional Environmental Change*, 15, 569-579.
- Newbold, T., Hudson, L., Hill, S., Contu, S., Lysenko, I., et al. (2015). Global effects of land use on local terrestrial biodiversity. *Nature*, 520, 45-50.
- Nicholls, N. (1995). Long-term climate monitoring and extreme events. *Climatic Change*, 31, 231-245.
- Oke, T. (1982). The energetic basis of the urban heat-island. *Quarterly Journal of the Royal Meteorological Society*, 108, 1-24.
- O'Neill, B., Tebaldi, C., van Vuuren, D., Eyring, V., Friedlingstein, P., et al. (2016). The Scenario Model Intercomparison Project (ScenarioMIP) for CMIP6. *Geoscientific Model Development*, 9, 3461-3482.
- Orlowsky, B., & Seneviratne, S. (2012). Global changes in extreme events: Regional and seasonal dimension. *Climatic Change*, 110, 669-696.
- Osborn, T., & Jones, P. (2014). The CRUTEM4 land-surface air temperature data set: Construction, previous versions and dissemination via Google Earth. *Earth System Science Data*, 6, 61-68.
- Perkins, S. (2015). A review on the scientific understanding of heatwaves - Their measurement, driving mechanisms, and changes at the global scale. *Atmospheric Research*, 164, 242-267.
- Perkins, S., Alexander, L., & Nairn, J. (2012). Increasing frequency, intensity and duration of observed global heatwaves and warm spells. *Geophysical Research Letters*, 39(L20714).
- Perkins-Kirkpatrick, S., & Gibson, P. (2017). Changes in regional heatwave characteristics as a function of increasing global temperature. *Scientific Reports*, 7(12256).
- Peterson, T., Hoerling, M., Stott, P., & Herring, S. (2013). Explaining extreme events of 2012 from a climate perspective. *Bulletin of the American Meteorological Society*, 94, S1-S74.
- Peterson, T., Stott, P., Herring, S., Zwiers, F., Hegerl, G., et al. (2012). Explaining extreme events of 2011 from a climate perspective. *Bulletin of the American Meteorological Society*, 93, 1041-1067.
- Pugh, T., Lindeskog, M., Smith, B., Poulter, B., Arneth, A., et al. (2019). Role of forest regrowth in global carbon sink dynamics. *Proceedings of the National Academy of Sciences of the United States of America*, 116, 4382-4387.
- Rahmstorf, S., & Coumou, D. (2011). Increase of extreme events in a warming world. *Proceedings of the National Academy of Sciences of the United States of America*, 108, 17905-17909.
- Robine, J., Cheung, S., Le Roy, S., Van Oyen, H., Griffiths, C., et al. (2008). Death toll exceeded 70,000 in Europe during the summer of 2003. *Comptes Rendus*

- Biologies*, 331, 171-178.
- Russo, S., Dosio, A., Graversen, R., Sillmann, J., Carrao, H., et al. (2014). Magnitude of extreme heat waves in present climate and their projection in a warming world. *Journal of Geophysical Research - Atmospheres*, 119, 12500-12515.
- Rusticucci, M. (2012). Observed and simulated variability of extreme temperature events over South America. *Atmospheric Research*, 106, 1-17.
- Santagata, D., Castesana, P., Rossler, C., & Gomez, D. (2017). Extreme temperature events affecting the electricity distribution system of the metropolitan area of Buenos Aires (1971-2013). *Energy Policy*, 106, 404-414.
- Searchinger, T., Wirseni, S., Beringer, T., & Dumas, P. (2018). Assessing the efficiency of changes in land use for mitigating climate change. *Nature*, 564, 249-253.
- Seland, Ø., Bentsen, M., Seland Graff, L., Olivié, D., Toniazzi, T., et al. (2020). The Norwegian Earth System Model, NorESM2 – Evaluation of the CMIP6 DECK and historical simulations. *Geoscientific Model Development*(submitted).
- Sellar, A., Jones, C., Mulcahy, J., Tang, Y., Yool, A., et al. (2019). UKESM1: Description and evaluation of the UK Earth System Model. *Journal of Advances in Modeling Earth Systems*, 11, 4513-4558.
- Semmler, T., Danilov, S., Gierz, P., Goessling, H., Hegewald, J., et al. (2020). Simulations for CMIP6 with the AWI climate model AWI-CM-1-1. *Journal of Advances in Modelling Earth Systems*, 12(e2019MS002009).
- Seneviratne, S., Donat, M., Pitman, A., Knutti, R., & Wilby, R. (2016). Allowable CO2 emissions based on regional and impact-related climate targets. *Nature*, 529, 477-483.
- Sillmann, J., Kharin, V., Zhang, X., Zwiers, F., & Bronaugh, D. (2013). Climate extremes indices in the CMIP5 multimodel ensemble: Part 1. Model evaluation in the present climate. *Journal of Geophysical Research - Atmospheres*, 118, 1716-1733.
- Sillmann, J., Kharin, V., Zwiers, F., Zhang, X., & Bronaugh, D. (2013). Climate extremes indices in the CMIP5 multimodel ensemble: Part 2. Future climate projections. *Journal of Geophysical Research - Atmospheres*, 118, 2471-2492.
- Stewart, I., & Oke, T. (2012). Local climate zones for urban temperature studies. *Bulletin of the American Meteorological Society*, 93, 1879-1900.
- Stott, P., Hegerl, G., Herring, S., Hoerling, M., Peterson, T., et al. (2014). Explaining extreme events of 2013 from a climate perspective. *Bulletin of the American Meteorological Society*, 95, S1-S96.
- Sun, Y., Zhang, X., Zwiers, F., Song, L., Wan, H., et al. (2014). Rapid increase in the risk to extreme summer heat in eastern china. *Nature Climate Change*, 4, 1082-1085.
- Swart, N., Cole, J., Kharin, V., Lazare, M., Scinocca, J., et al. (2019). The Canadian Earth System Model version 5 (CanESM5.0.3). *Geoscientific Model Development*, 12, 4823-4873.
- Tatebe, H., Ogura, T., Nitta, T., Komuro, Y., Ogochi, K., et al. (2019). Description and basic evaluation of simulated mean state, internal variability, and climate sensitivity in MIROC6. *Geoscientific Model Development*, 12, 2727-2765.
- Taylor, K., Stouffer, R., & Meehl, G. (2012). An overview of CMIP5 and the experiment design. *Bulletin of the American Meteorological Society*, 93, 485-498.
- Tebaldi, C., & Knutti, R. (2007). The use of the multi-model ensemble in probabilistic climate projections. *Philosophical Transactions of the Royal Society A - Mathematical Physical and Engineering Sciences*, 365, 2053-2075.
- Tranter, B. (2011). Political divisions over climate change and environmental issues in Australia. *Environmental Politics*, 20, 78-96.
- Viceto, C., Pereira, S., & Rocha, A. (2019). Climate change projections of extreme temperatures for the Iberian Peninsula. *Atmosphere*, 10(229).

- Visser, H., & Petersen, A. (2012). Inferences on weather extremes and weather-related disasters: A review of statistical methods. *Climate of the Past*, 8, 265-286.
- Voldoire, A., Saint-Martin, D., Senesi, S., Decharme, B., Alias, A., et al. (2019). Evaluation of CMIP6 DECK experiments with CNRM-CM6-1. *Journal of Advances in Modeling Earth Systems*, 11, 2177-2213.
- Volodin, E., Mortikov, E., Kostykin, S., Galin, V., Lykosov, V., et al. (2017). Simulation of modern climate with the new version of the INM RAS climate model. *Izvestiya Atmospheric and Oceanic Physics*, 53, 142-155.
- Volodin, E., Mortikov, E., Kostykin, S., Galin, V., Lykosov, V., et al. (2018). Simulation of the modern climate using the INM-CM48 climate model. *Russian Journal of Numerical Analysis and Mathematical Modelling*, 33, 367-374.
- Wang, J., Chen, Y., Tett, S., Yan, Z., Zhai, P., et al. (2020). Anthropogenically-driven increases in the risks of summertime compound hot extremes. *Nature Communications*, 11(528).
- Wernberg, T., Smale, D., Tuya, F., Thomsen, M., Langlois, T., et al. (2013). An extreme climatic event alters marine ecosystem structure in a global biodiversity hotspot. *Nature Climate Change*, 3, 78-82.
- Wigley, T. (1985). Climatology - Impact of extreme events. *Nature*, 316, 106-107.
- Wigley, T. (2009). The effect of changing climate on the frequency of absolute extreme events. *Climatic Change*, 97, 67-76.
- Wu, T., Lu, Y., Fang, Y., Xin, X., Li, L., et al. (2019). The Beijing Climate Center Climate System Model (BCC-CSM): The main progress from CMIP5 to CMIP6. *Geoscientific Model Development*, 12, 1573-1600.
- Yukimoto, S., Kawai, H., Koshiro, T., Oshima, N., Yoshida, K., et al. (2019). The Meteorological Research Institute Earth System Model version 2.0, MRI-ESM2.0: Description and basic evaluation of the physical component. *Journal of the Meteorological Society of Japan*, 97, 931-965.
- Zhang, D., Huang, Q., He, C., & Wu, J. (2017). Impacts of urban expansion on ecosystem services in the Beijing-Tianjin-Hebei urban agglomeration, China: A scenario analysis based on the Shared Socioeconomic Pathways. *Earth System Dynamics*, 9, 115-130.